

# Bayesian Inference of General Noise Model Parameters from Surface Code's Syndrome Statistics

Takumi Kobori\*

*Department of Physics, The University of Tokyo, Tokyo 113-0033, Japan*

Synge Todo†

*Department of Physics, The University of Tokyo, Tokyo 113-0033, Japan*

*Institute for Physics of Intelligence, The University of Tokyo, Tokyo 113-0033, Japan and*

*Institute for Solid State Physics, The University of Tokyo, Kashiwa, 277-8581, Japan*

(Dated: August 1, 2024)

Active research on the surface code shows that its decoding performance can be significantly enhanced by utilizing the information of the noise model and optimizing the grid shape and decoding algorithm. Usually, the parameters in the noise model for the quantum error correction code must be prepared separately using some method, such as the quantum process tomography. There is a strong need to perform noise model estimation in parallel with the syndrome measurement during decoding to avoid the demanding prior tomography procedure. While noise model estimation based on syndrome measurement statistics is well-explored for Pauli noise, it remains under-studied for more complex noise models like amplitude damping. In this paper, we propose general noise model Bayesian inference methods that integrate the surface code's tensor network simulator, which can efficiently simulate various noise models, with Monte Carlo sampling techniques. For stationary noise, where the noise parameters are constant and do not change, we propose a method based on the Markov chain Monte Carlo. For time-varying noise, which is a more realistic situation, we introduce another method based on the sequential Monte Carlo. We present the numerical results of applying the proposed methods to various noise models, such as static, time-varying, and non-uniform cases, and evaluate their performance in detail.

## I. INTRODUCTION

Since the first proposal by Feynman [1], the field of quantum computers has grown significantly and is now considered new-generation computers [2]. Their realization is expected to enable faster computations than classical computers for several tasks [3–5]. Their calculations are performed using qubits, which are quantum-mechanical bits. Thanks to the properties of quantum mechanics, qubits can allow them to perform calculations more efficiently than classical computers. Unfortunately, information stored on qubits is so fragile that executing stable calculations with them is challenging. The vulnerability arises from a lack of focus on noise elimination, which is difficult to avoid due to the need for external control of the qubits during computation. The quantum error correction (QEC) codes [6] were proposed to deal with the noisy qubits under a solid demand for realizing fault-tolerant quantum computers (FTQC). The QEC codes can correct the errors caused by the noise and can achieve error-free quantum computation.

Among several QEC codes, the surface code [7–9] is considered one of the most promising candidates for future quantum computers, especially near-term FTQC. Thanks to its geometrical properties, it exhibits high performance and is easy to implement on 2D chips. This is why so much research is being done to make it realized.

Some papers have reported the successful experimental implementation of the surface code using the superconducting qubits [10, 11] or neutral-atom qubits [12].

The surface code has been studied very intensively, not only experimentally but also theoretically. There have been many proposals to improve its performance from the viewpoint of the grid shape and decoder. In particular, the performance of the decoding algorithm can be improved by using noise model information [13–16]. In addition, the grid shape and the Clifford deformation of its stabilizer generators affect its code performance [17–20]. Thus, the surface code performance is significantly improved by optimization based on the noise model information.

Such noise model knowledge is usually prepared in advance by performing quantum process tomography [21, 22], where the quantum computer has to be operated aside from the main calculations. In addition, there is a problem with time-varying noise models. If the noise model changes over time, one has to update the noise model information by performing additional operations. There is a strong need to perform noise model estimation in parallel with the syndrome measurement during the decoding process, as we can avoid the demanding prior tomography procedure or perform online learning of noise model parameters that change over time. Although there have been some attempts at the noise model estimation based on syndrome statistics, only the Pauli noise model case has been considered so far [23–25]. In particular, its estimability has been discussed precisely in Ref. [26]. For the time-varying noise model, the online estimation of

\* [takumi.kobori@phys.s.u-tokyo.ac.jp](mailto:takumi.kobori@phys.s.u-tokyo.ac.jp)

† [wisteria@phys.s.u-tokyo.ac.jp](mailto:wisteria@phys.s.u-tokyo.ac.jp)

the Pauli channel has also been studied actively [13, 27]. An experimental study for online estimation was also reported in Ref. [28].

There are several reasons why Pauli noise estimation is being actively studied. First, both Pauli noise and stabilizer code simulations can be efficiently performed using stabilizer methods, which work in polynomial time with respect to the number of qubits on classical computers [29, 30]. Second, the general noise model can be projected to the Pauli noise by randomized compiling [31]. However, it is crucial to consider general noise models, not merely Pauli noise models, as randomized compiling requires additional circuit execution and knowledge of the general noise models benefits decoders that utilize this information.

An efficient simulation method for the surface code is required to estimate general noise models effectively. To go beyond the Pauli noise model, we focus on tensor network (TN) simulation. This technique allows us to simulate the surface code with a general noise model in  $O(\#qubits)$  by introducing the low-rank tensor approximation [20]. In addition, we can also calculate the likelihood function  $p(\mathbf{S}|\boldsymbol{\alpha})$  efficiently in the TN formulation, where  $\mathbf{S}$  are the outcomes of syndrome measurements and  $\boldsymbol{\alpha}$  are the parameters in the parameterized noise model. By utilizing the efficient likelihood calculation provided by TN simulation, effective general noise model estimation can be achieved. In the previous work [25], they proposed the estimation method that uses the brief propagation to calculate the likelihood function and the EM algorithm [32], one of the maximum likelihood estimation methods. Unfortunately, the belief propagation only applies to the Pauli noise models, and so does their estimation method based on it.

We attempt to overcome the limitations above by estimating noise models using Bayesian inference [33]. Bayesian inference is an estimation based on the posterior distribution,  $p(\boldsymbol{\alpha}|\mathbf{S})$ , which is calculated via Bayes' theorem,  $p(\boldsymbol{\alpha}|\mathbf{S}) \propto p(\mathbf{S}|\boldsymbol{\alpha})p(\boldsymbol{\alpha})$ , where  $p(\boldsymbol{\alpha})$  is a prior distribution. Although obtaining the posterior distribution in an analytic form is generally tricky, we can generate samples according to the posterior distribution without bias using the Monte Carlo sampling methods. For the data set prepared before the simulation, the Markov chain Monte Carlo (MCMC) is the method to be used [34–36]. If the data is to be generated sequentially, on the other hand, the sequential Monte Carlo method (SMC) is more suitable [37, 38]. Thanks to the Monte Carlo sampling methods, Bayesian inference is increasingly used in many fields [33]. In estimating the general noise model, Bayesian inference can be effectively employed through Monte Carlo methods by calculating the likelihood function using TN simulation.

In the present paper, we propose novel noise Bayesian inference methods based on syndrome statistics for general noise models in the surface code. We consider two different cases: the stationary noise model and the time-varying noise model. For the stationary noise case, where

the noise parameters are constant and do not change, we propose a method based on MCMC. For the time-varying noise case, which is a more realistic situation, we introduce the method using SMC. We report the results of several noise models beyond the Pauli noise models. We find that the estimation for many cases, such as the amplitude damping, works quite successfully, but for some cases, such as the generalized amplitude damping noise model, it does not. We also demonstrate that applying the results of the noise model estimation to the TN decoder improves its performance.

The rest of the present paper is organized as follows: In Sec. II, we briefly review the stabilizer code and surface code. Then, we review a TN simulation of the surface code. In Sec. III, we explain how to estimate the noise model parameters using Bayesian inference and our proposed method based on the TN simulation and the Monte Carlo methods. In Sec. IV, we show the numerical results of the proposed methods and discuss their efficiency and estimability. In Sec. V, we summarize the present paper and future issues.

## II. PRELIMINARY AND TENSOR NETWORK SIMULATION OF SURFACE CODE

### A. Stabilizer code

The stabilizer code [39] is characterized by a stabilizer group and stabilizer generators. The stabilizer group is defined as the abelian subgroup of the Pauli group:

$$\begin{aligned} \mathcal{S} = \{S_i\} \in \mathcal{P}_n \\ \text{s.t. } -I \notin \mathcal{S} \text{ and } \forall S_i, S_j \in \mathcal{S}, [S_i, S_j] = 0. \end{aligned} \quad (1)$$

A stabilizer group has generators, which are called stabilizer generators. To consider the stabilizer group, it is essential to focus on stabilizer generators. A stabilizer group can label some quantum states in restricted Hilbert spaces. They are called the stabilizer states. A stabilizer state  $|\psi\rangle$ , defined by the stabilizer group  $\mathcal{S}$ , satisfies the following property:

$$\forall S_i \in \mathcal{S}, S_i |\psi\rangle = |\psi\rangle. \quad (2)$$

In other words, the stabilizer states  $|\psi\rangle$  are +1 eigenstates of any element of the stabilizer group. Due to the commutation relations among stabilizers, a state qualifies as a stabilizer state of the group if and only if all eigenvalues of the stabilizer generators are +1. Therefore, the above definition is rewritten in terms of the set of stabilizer generators  $\mathcal{S}_g$  as

$$\forall g_i \in \mathcal{S}_g, g_i |\psi\rangle = |\psi\rangle. \quad (3)$$

The dimension of the Hilbert space of stabilizer states is  $2^{n-|\mathcal{S}_g|}$  for the  $n$ -qubit case where  $|\mathcal{S}_g|$  means the number of stabilizer generators.

Similar to general quantum codes, original states must be encoded within the stabilizer code framework. The

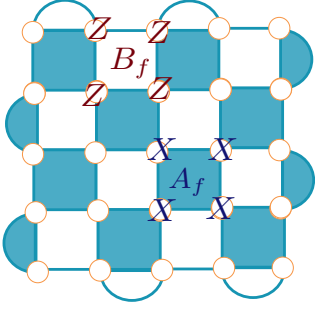


FIG. 1: Rotated surface code with  $d = 5$ . The number of physical qubits and stabilizer generators is 25 and 24, respectively. This figure only shows the physical qubits but not the qubits for syndrome measurements.

encoded code states are defined by the stabilizer states, and the code space is the Hilbert space restricted by the stabilizers. The code states  $|\psi\rangle$  and code space  $\mathcal{C}$  are defined as the

$$|\psi\rangle \in \mathcal{C} \iff \forall g_i \in \mathcal{S}_g, g_i |\psi\rangle = |\psi\rangle. \quad (4)$$

If the number of stabilizer generators is  $n - k$ , the dimension of the restricted Hilbert space of the stabilizer code is  $2^k$ . Therefore, the code states can represent  $k$  logical qubits, which encode the original  $k$ -qubit states.

To correct the error, we have to get some information from codes. We focus on the parity change in the eigenvalues of stabilizer generators so as not to destroy the quantum states after measurements. Such parity check measurements are called syndrome measurements. The syndrome measurements are executed using one ancilla qubit for each stabilizer generator. The decoding process of the stabilizer code is as follows:

1. Error detection: Obtain the results of the syndrome measurement of the stabilizer generators.
2. Error estimation: Based on the results, the decoding algorithm calculated by a classical computer is used to estimate where the error occurred.
3. Error correction: Based on the estimated errors, correct the error by operating to erase the errors or update the Pauli frame [40].

### B. Surface code

The surface code, a type of stabilizer code, is a leading candidate for QEC in future FTQC due to its high performance. One type of surface code is represented like Fig. 1 [41]. Its stabilizer generators can be written by only the product of  $X$  or  $Z$ . In Fig. 1, the blue area represents the product of  $X$ , and the white area represents the product of  $Z$ . Let the lattice be  $L \times W$ , and its code distance is  $d = \min(L, W)$ , which means the code can detect the  $d - 1$  errors. The number of qubits is  $LW$  to

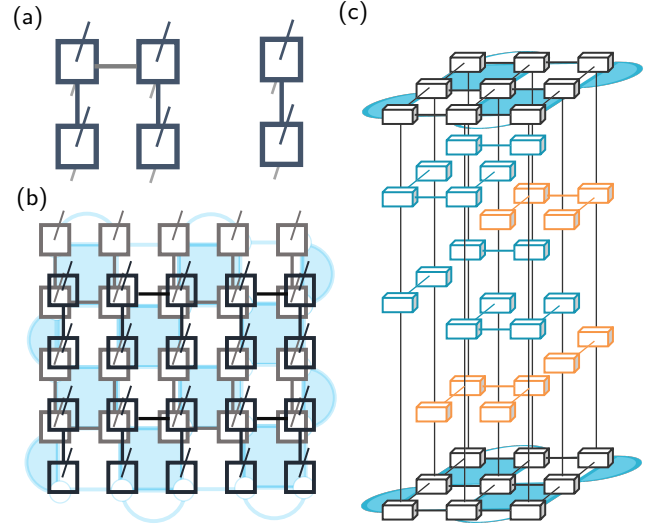


FIG. 2: (a) TN representation of projectors  $\Pi_{\pm g} = (I \pm g)/2$ . (b) TN representation of  $d = 5$  initial code state  $|0\rangle_L^{\otimes 25}$ . It can be made from  $|0\rangle_L^{\otimes 25}$  by operating the  $X$  stabilizer projectors. It is because  $|0\rangle_L^{\otimes 25}$  is already stabilized by the products of  $Z$ . (c) A conceptual picture of the TN diagram of the likelihood  $p(\mathbf{m}|\boldsymbol{\alpha})$  calculation of  $d = 3$  surface code.

represent the code and  $LW - 1$  for ancilla qubits used in syndrome measurements. Their stabilizer generators are represented by the product of two or four Pauli operators, and the physical qubit on which they act is spatially localized. Consequently, the surface code can be implemented with qubits arranged in a two-dimensional grid, where operations are performed on adjacent qubits. That is why we can simulate them using the TN efficiently.

### C. Tensor network simulation of surface code

The TN simulation is one of the most valuable and powerful numerical methods [42]. It is the method for efficiently compressing the Hilbert space of quantum systems. To represent the state of quantum many-body systems, tensors, which are multidimensional arrays, are used and connected by contraction in the TN. By using the representative class of TNs, PEPS [43] and MPS-MPO [44], the surface code can be simulated efficiently [20].

To simulate the surface code, TN representation of the projector onto the eigenspace of  $\pm 1$  eigenvalue of stabilizer generators is needed. It can be written as  $(I \pm g)/2$  for each stabilizer generator  $g$ , and it is represented by the tensors with bond dimension two as shown in Fig. 2(a). When we label the horizontal leg indices by  $\alpha$ , the TN represent the product of  $I$  for  $\alpha = 0$ ,  $X$  or  $Z$  for  $\alpha = 1$ , and zero otherwise. All legs have bond dimension 2, so the representation is very efficient.

By using the projectors  $\Pi_{\pm g} = (I \pm g)/2$  for  $g \in \mathcal{S}_g$ ,

we can represent the initial code states  $|0\rangle_L$ , and conduct syndrome measurements (see Fig. 2). The whole process of surface code simulation can be written as  $\mathcal{D} \circ \mathcal{S} \circ \mathcal{E}(\rho_0)$ , where  $\rho_0$  is the initial code state such as  $|0\rangle_L \langle 0|$ ,  $\mathcal{E}$  is the noise process,  $\mathcal{S}$  is the process of syndrome measurements, and  $\mathcal{D}$  is the decoding process. The noise process  $\mathcal{E}$  can be represented as the CPTP map of the density matrix and the process can be represented by the tensor. The decoding process  $\mathcal{D}$  is the Pauli operation and can also be represented by the tensor easily.

The syndrome measurement process  $\mathcal{S}$  can be considered the projection onto the eigenspace of each stabilizer generator. Therefore, they are represented by the projector  $\Pi_{\pm g}$ . By using these projectors, measurement qubits can be omitted. Each syndrome measurement can be executed by calculating  $p_{+g} = \text{Tr}(\Pi_{+g}\rho\Pi_{+g}) = \text{Tr}(\Pi_{+g}\rho)$ , which gives the probability of +1 eigenvalue.  $\text{Tr}(\Pi_{+g}\rho)$  is calculated by the contracting the whole TNs. By using a random number of uniform distribution from 0 to 1, we can choose +1 state or -1 state, and then we recalculate  $\rho \leftarrow \Pi_{+g}\rho$  or  $\rho \leftarrow \Pi_{-g}\rho$ . By repeating the calculation for all  $g \in \mathcal{S}_g$ , the syndrome measurements are completed, and we obtain the syndrome measurement outcomes  $\mathbf{S}$  where  $S_i$  is the syndrome measurement outcome of the  $i$ th stabilizer generator  $g_i$ .

Applying this calculation method, we can obtain the likelihood function  $p(\mathbf{S}|\boldsymbol{\alpha})$  where  $\boldsymbol{\alpha}$  are the parameters representing the noise models  $\mathcal{E}_{\boldsymbol{\alpha}}$ . The likelihood function is expressed as  $p(\mathbf{S}|\boldsymbol{\alpha}) = \text{Tr}(\prod_i \Pi_{S_i g_i} \mathcal{E}_{\boldsymbol{\alpha}}(\rho_0))$  so it can be calculated by the TN by preparing the TN representing the initial code state, contracting the tensor representing noise process  $\mathcal{E}_{\boldsymbol{\alpha}}$  and the whole projector tensors corresponding to the measurement outcomes  $\mathbf{m}$ , and contracting whole TN like Fig. 2(c).

In the present formulation, we have to be aware of some points. It is assumed that the syndrome measurements are perfect noise-less syndrome measurements. In the real devices, noise is also applied to the syndrome measurement of ancilla qubits. So, it can be said that the present simulation is simplified by neglecting noise for syndrome measurements. While, if we think about noise for syndrome measurements, the noise simulations are more complicated; for example, the order of control gates of syndrome measurements has to be considered as in Ref. [45].

The time complexity for the exact calculation of the whole TN by PEPS is  $O(d^2 4^d)$ . For large-scale surface code, we have to introduce some approximation. By initially contracting physical bonds, the TN forms a 2D square network, allowing us to use the boundary MPS-MPO. The approximation time complexity is  $O(d^2 \chi^3)$ , for  $\chi$  being the maximum bond dimension. Thus, we can simulate the surface code almost linearly to the number of qubits. This simulator has been applied for the decoding algorithm [16, 46], and we used it to evaluate the improvement of decoding performance by our noise model estimator. This simulator can handle not only the Pauli noise but also arbitrary noise, so this simulator can

also be applied to our method of quantum noise model estimation.

### III. THE METHODS

#### A. Bayesian inference of noise model based on syndrome measurements

First, we have to set objective functions to perform estimations. In our case, the results of syndrome measurements,  $\mathbf{S}_{0:n-1} = \{\mathbf{S}_0, \mathbf{S}_1, \dots, \mathbf{S}_{n-1}\}$ , are only the information we have. Here,  $n$  is the number of cycles of syndrome measurements, and  $\mathbf{S}_i$  is the set of one cycle syndrome measurement results, so if we consider  $L \times W$  surface code, the number of elements in  $\mathbf{S}_i$  is  $L \times W - 1$ . The noise model is parameterized by a set of parameters,  $\boldsymbol{\alpha}$ , even in the case of general noise models. From the viewpoint of Bayesian inference, estimation is performed using the conditional probability distribution  $p(\boldsymbol{\alpha}|\mathbf{S}_{0:n-1})$ . The conditional probability  $p(\boldsymbol{\alpha}|\mathbf{S}_{0:n-1})$  is also called the posterior distribution in Bayesian inference. We calculate the posterior distribution using the Bayes' theorem:

$$\begin{aligned} p(\boldsymbol{\alpha}|\mathbf{S}_{0:n-1}) &= \frac{p(\mathbf{S}_{0:n-1}|\boldsymbol{\alpha})p(\boldsymbol{\alpha})}{p(\mathbf{S}_{0:n-1})} \\ &= \frac{p(\mathbf{S}_{0:n-1}|\boldsymbol{\alpha})p(\boldsymbol{\alpha})}{\int d\boldsymbol{\alpha} p(\mathbf{S}_{0:n-1}|\boldsymbol{\alpha})p(\boldsymbol{\alpha})} \\ &\propto p(\mathbf{S}_{0:n-1}|\boldsymbol{\alpha})p(\boldsymbol{\alpha}), \end{aligned} \quad (5)$$

where  $p(\boldsymbol{\alpha})$  is the prior distribution and  $p(\mathbf{S}_{0:n-1}|\boldsymbol{\alpha})$  is the likelihood function. In the Bayesian inference, we initially set the prior distribution  $p(\boldsymbol{\alpha})$ , and by multiplying this with the likelihood  $p(\mathbf{S}_{0:n-1}|\boldsymbol{\alpha})$ , we refine the posterior function and enhance the estimation results. The prior distribution is chosen as the limited-range uniform distribution to avoid unphysical solutions.

After calculating the posterior distribution, we can analyze the estimation results by observing the whole landscape of the distribution or statistics computed from the distribution. We have several choices for statistics, but we chose the expected a posterior (EAP) estimator for evaluating results, which is defined as  $\boldsymbol{\alpha}^* = \int d\boldsymbol{\alpha} \boldsymbol{\alpha} p(\boldsymbol{\alpha}|\mathbf{S}_{0:n-1})$ .

#### B. Markov chain Monte Carlo for stationary noise model

In practical situations, the posterior distribution  $p(\boldsymbol{\alpha}|\mathbf{S})$  cannot be evaluated analytically. So, we have to rely on sampling methods, such as the MCMC, to calculate them. It is particularly useful for Bayesian inference as we can sample from the posterior distributions. The most famous MCMC method is the Metropolis-Hastings (M-H) algorithm [34]. The M-H algorithm enables us



to perform sampling from an unnormalized distribution function. In the context of Bayesian inference, we can sample from the posterior distribution without knowing the normalization factor,  $P(\mathbf{S}_{0:n-1})$ .

For estimating the noise model based on the syndrome statistics of QEC by Bayesian inference, the likelihood  $p(\mathbf{S}|\boldsymbol{\alpha})$  must be calculated. In our methods, we calculate the likelihood using the TN simulation. Generally, the time complexity of approximate TN calculation is  $O(\#qubits)$ , so the Bayesian inferences are efficient. In the present paper, we used the simulator Sec. II C for the surface code. The whole algorithm is given in Alg. 1.

---

**Algorithm 1** Bayesian inference using MCMC for stationary noise model

---

**Input:** results of syndrome  $\mathbf{S}_{0:n-1}$ , burn-in-time  $s$ , total MC steps  $T$  ( $> s$ ), prior distribution  $p(\boldsymbol{\alpha})$ , proposal distribution  $q(\boldsymbol{\alpha}', \boldsymbol{\alpha})$ , max bond dimension of TN  $\chi$

**Output:** samples of  $p(\boldsymbol{\alpha}|\mathbf{S}_{0:n-1})$

- 1: Initialize  $\boldsymbol{\alpha}^0 \sim p(\boldsymbol{\alpha})$
- 2: Likelihood  $p(\mathbf{S}_{0:n-1}|\boldsymbol{\alpha}^0) \leftarrow TNsimulator(\mathbf{S}_{0:n-1}, \boldsymbol{\alpha}^0, \chi)$
- 3: **for**  $i = 0, 1, \dots, T$  **do**
- 4:   Sample  $\boldsymbol{\alpha}' \sim q(\boldsymbol{\alpha}', \boldsymbol{\alpha}^i)$
- 5:   Likelihood  $p(\mathbf{S}_{0:n-1}|\boldsymbol{\alpha}') \leftarrow TNsimulator(\mathbf{S}_{0:n-1}, \boldsymbol{\alpha}', \chi)$
- 6:    $\gamma \leftarrow \min\left(1, \frac{p(\mathbf{S}_{0:n-1}|\boldsymbol{\alpha}')}{p(\mathbf{S}_{0:n-1}|\boldsymbol{\alpha}^i)}\right)$
- 7:   Sample  $r \sim \text{Uniform}(r; 0, 1)$
- 8:   **if**  $r < \gamma$  **then**
- 9:      $\boldsymbol{\alpha}^{i+1} \leftarrow \boldsymbol{\alpha}'$
- 10:     $p(\mathbf{S}_{0:n-1}|\boldsymbol{\alpha}^{i+1}) \leftarrow p(\mathbf{S}_{0:n-1}|\boldsymbol{\alpha}')$
- 11:   **else**
- 12:      $\boldsymbol{\alpha}^{i+1} \leftarrow \boldsymbol{\alpha}^i$
- 13:     $p(\mathbf{S}_{0:n-1}|\boldsymbol{\alpha}^{i+1}) \leftarrow p(\mathbf{S}_{0:n-1}|\boldsymbol{\alpha}^i)$
- 14: **return**  $\{\boldsymbol{\alpha}^s, \boldsymbol{\alpha}^{s+1}, \dots, \boldsymbol{\alpha}^T\}$

---

In this algorithm, we set the proposal distribution as  $q(\boldsymbol{\alpha}', \boldsymbol{\alpha}) = q(\boldsymbol{\alpha}, \boldsymbol{\alpha}')$  so that the detailed balance condition is satisfied. This method can be applied to more general noise models than Pauli noise models, as the likelihood can be calculated by the TN simulator.

There are some points to note for our MCMC and TN methods. One is that the MCMC samples suffer from autocorrelation, unlike perfect sampling. So, we have to thin out samples or collect many samples. Because of the correlation time, the calculation may take longer than the direct methods like [26]. They use the characterization of the stabilizer code and Pauli noise models directly, so the estimation is more direct and faster than our MCMC method. However, it should be emphasized that our MCMC method can estimate the Pauli noise model and general noise models thanks to the efficient TN simulators. It is one of the most significant advantages of our proposed methods. Second is the error in the estimates. For MCMC, there are some statistical errors. Furthermore, for TN, there is a truncation error in the approximate contraction of the TN. So, to evaluate the accuracy of the estimates, we have to consider both of them. Third, the MCMC method is not suitable for

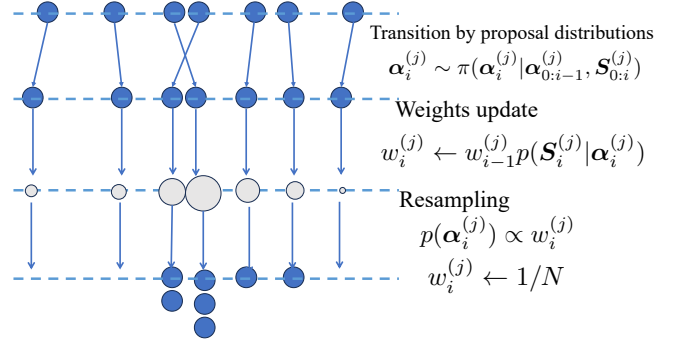


FIG. 3: Conceptual diagram of updates of weighted particles for one cycle results in SMC.

the time-varying noise models. In quantum noise model estimation based on syndrome measurements, estimating time-varying noise model adaptively is more valuable. To deal with them, we developed another method based on the SMC, which is discussed below.

### C. Sequential Monte Carlo for time-varying noise model

In QEC, we can get results of syndrome measurements sequentially. The form of QEC and the decode performance are influenced very much by the information of the noise model. However, in realistic situations, the noise models vary over time. So, continuously updating the noise model information is essential to improve QEC. Such sequential estimations can be realized by the SMC [37, 38, 47]. SMC is also called the particle filter. We explain SMC and its application for noise model estimation below.

First, we explain the problem setting. For the time-varying case, the noise model parameters are described as  $\{\boldsymbol{\alpha}_0, \boldsymbol{\alpha}_1, \dots, \boldsymbol{\alpha}_{n-1}\}$ . Syndrome measurements  $\mathbf{S}_i$  can be obtained sequentially which are generated according to  $p(\mathbf{S}_i|\boldsymbol{\alpha}_i)$ . Our goal is to estimate the latest  $\boldsymbol{\alpha}_i$  based on the previous syndrome measurement results  $\mathbf{S}_{0:i} = \{\mathbf{S}_0, \mathbf{S}_1, \dots, \mathbf{S}_i\}$ . In the Bayesian inference, we calculate the posterior distribution  $p(\boldsymbol{\alpha}_{0:i}|\mathbf{S}_{0:i})$  and the marginal distribution  $p(\boldsymbol{\alpha}_i|\mathbf{S}_{0:i})$  to estimate  $\boldsymbol{\alpha}_i$ .

To simulate the posterior distribution continuously, we use the SMC.

In the SMC, we use the weighted particles by representing the posterior distribution  $p(\boldsymbol{\alpha}_{0:i}|\mathbf{S}_{0:i})$  as a product of weight function  $w(\boldsymbol{\alpha}_{0:i})$  and posterior function  $\pi(\boldsymbol{\alpha}_{0:i}|\mathbf{S}_{0:i})$  like

$$p(\boldsymbol{\alpha}_{0:i}|\mathbf{S}_{0:i}) = w(\boldsymbol{\alpha}_{0:i})\pi(\boldsymbol{\alpha}_{0:i}|\mathbf{S}_{0:i}). \quad (6)$$

So, if we simulate  $N$  particles  $\{\boldsymbol{\alpha}_{0:i}^{(j)}\}$  ( $j = 1, \dots, N$ ) sampled from  $\pi(\boldsymbol{\alpha}_{0:i}|\mathbf{S}_{0:i})$  according to the weight  $w(\boldsymbol{\alpha}_{0:i})$ , the posterior distribution  $p(\boldsymbol{\alpha}_{0:i}|\mathbf{S}_{0:i})$  can be approximated by weighted particles.

We try to simulate such  $N$  particles with weight  $w$ . We can recursively calculate the proposal distribution as follows:

$$\begin{aligned}\pi(\alpha_{0:i}|\mathbf{S}_{0:i}) &= \pi(\alpha_{0:i-1}|\mathbf{S}_{0:i-1})\pi(\alpha_i|\alpha_{0:i-1}, \mathbf{S}_{0:i}) \\ &= \pi(\alpha_0) \prod_{j=0}^{i-1} \pi(\alpha_{j+1}|\alpha_{0:j}, \mathbf{S}_{0:j+1}).\end{aligned}\quad (7)$$

The importance weight  $w(\alpha_{0:i})$  will be

$$\begin{aligned}w(\alpha_{0:i}) &= \frac{p(\alpha_{0:i}|\mathbf{S}_{0:i})}{\pi(\alpha_{0:i}|\mathbf{S}_{0:i})} \\ &\propto w(\alpha_{0:i-1}) \frac{p(\mathbf{S}_i|\alpha_i)p(\alpha_i|\alpha_{i-1})}{\pi(\alpha_i|\alpha_{0:i-1}, \mathbf{S}_{0:i})}.\end{aligned}\quad (8)$$

This allows for rapid calculation of weights using the likelihood.

To consider such a sequential weight update, we have to deal with excessive weight degeneracy. In SMC, there is a well-known approach, resampling. There are four famous resampling methods: the multinomial, stratified, systematic, and residual resampling [47–51]. Their time complexities are  $O(N)$  or  $O(N \log N)$ . Among various resampling methods, the recommendation for the first choice is systematic resampling because it exhibits good performance in many cases [52, 53]. In the present work, we mainly use the systematic resampling method. The systematic resampling algorithm is given in Alg. 2.

---

#### Algorithm 2 Systematic resampling

---

**Input:** weights  $\{w^{(j)}\}$ , samples  $\{\mathbf{x}^{(j)}\}$

**Output:** samples  $\{\mathbf{x}'^{(j)}\}$

- 1: Cumulative sum of  $\{w^{(j)}\}$   $\{C^j\}$
  - 2: Number of samples  $n$ , Systematic choice  $u_0 \sim \text{Uniform}(u; 0, 1/n)$
  - 3: Index  $i \leftarrow 0, j \leftarrow 0$
  - 4: **while**  $i < n$  **do**
  - 5:     **while**  $C^j < u_0 + i/n$  **do**
  - 6:          $j \leftarrow j + 1$
  - 7:          $\mathbf{x}'^i \leftarrow \mathbf{x}^j$
  - 8:          $i \leftarrow i + 1$
  - 9: **return**  $\{\mathbf{x}'^{(j)}\}$
- 

SMC is also called the particle filter. Its conceptual diagram is shown in Fig. 3 for easy understanding. If the proposal distribution  $\pi(\alpha_i|\alpha_{0:i-1}, \mathbf{S}_{0:i})$  equals to the prior distribution  $p(\alpha_i|\alpha_{i-1})$ , the weight will be  $w(\alpha_{0:i}) \propto w(\alpha_{0:i-1})p(\mathbf{S}_i|\alpha_i)$  and we can calculate the weight by only using the likelihood. Such a choice of proposal distribution is called a bootstrap filter and is often used in realistic situations. The bootstrap filter [54, 55] is also used in our method.

Our method for estimating time-varying noise is based on SMC and the bootstrap filter. To use the bootstrap filter, we must choose the proposal distribution according to the system models of applied noise. The noise model parameters are expected to be stable thanks to the experimental effort. Setting the random walk distribution

as the proposal distribution is appropriate for stable parameter estimations. Such random walk proposal distribution is often used to track the objective parameter that moves relatively tiny.

---

#### Algorithm 3 Bayesian inference using SMC for time-varying noise model

---

**Input:** results of syndrome  $\mathbf{S}_{0:n-1}$ , resampling interval  $T$ , number of particles  $N$ , smoothing time  $t$ , proposal distribution  $q(\alpha', \alpha)$ , prior distribution  $p(\alpha)$ , max bond dimension of TN  $\chi$

**Output:** estimated parameters  $\{\bar{\alpha}_i\}$

- 1: Initialize  $N$  particles from prior distribution  $\{\alpha_0^{(j)}\} \sim p(\alpha)$
  - 2: Initialize weights  $\{w_0^{(j)} \leftarrow 1/N\}$
  - 3: EAP estimator  $\alpha^{EAP}_0 \leftarrow \text{WeightedMean}(\{\alpha_0^{(j)}\}, \{w_0^{(j)}\})$
  - 4: **for**  $i = 1, \dots$  **do**
  - 5:     **for**  $j = 0, 1, \dots, N$  **do**
  - 6:         Sample  $\alpha_i^{(j)} \sim q(\alpha_i^{(j)}, \alpha_{i-1}^{(j)})$
  - 7:          $w_i^{(j)} \leftarrow w_{i-1}^{(j)} \text{TNsimulator}(\mathbf{S}_i, \alpha_i^{(j)}, \chi)$
  - 8:     **if**  $i \% T = 0$  **then**
  - 9:         Normalize weights  $\{w_i^{(j)}\} \leftarrow \text{Normarize}(\{w_i^{(j)}\})$
  - 10:         resampling  $\{\alpha_i^{(j)}\} \leftarrow \text{Resample}(\{\alpha_i^{(j)}\}, \{w_i^{(j)}\})$
  - 11:         Update weights  $\{w_i^{(j)} = 1/N\}$
  - 12:     EAP estimator  $\alpha^{EAP}_i \leftarrow \text{WeightedMean}(\{\alpha_i^{(j)}\}, \{w_i^{(j)}\})$
  - 13:     Estimator  $\bar{\alpha}_i \leftarrow \text{Mean}(\{\alpha^{EAP}_{\max(0, i-t+1)}, \dots, \alpha^{EAP}_i\})$
  - 14: **return**  $\{\bar{\alpha}_i\}$
- 

SMC has several advantages. One of them is the ease of implementing parallel computing. We can trivially parallelize the updating process of SMC by distributing particles to many processors. On the other hand, the resampling process requires communication between processors. Optimizing the interval for resampling based on some criterion unlike Fig. 3 is recommended for efficiency. An effective particle number is often used for the criterion of resampling, but it requires additional communication between processes. In the present simulation, we use a constant resampling interval instead of the effective particle number.

Additionally, the sampling bias inherent in syndrome measurements impacts the accuracy of our estimations. The relation between syndrome measurements and noise models is not simple and probabilistic. To reduce the sampling bias, we must accumulate many results from the syndrome measurement. For that purpose, we introduce smoothing processes using near-past data: The estimate is evaluated by not only the EAP estimator of the latest particles but also the near-past EAP estimators. To sum up, our method based on the bootstrap filter is described in Alg. 3.

## IV. NUMERICAL EXPERIMENTS

In this section, we show the results of numerical experiments with our proposed method, the Bayesian noise model estimation based on the TN simulation of the surface code, and the Monte Carlo sampling technique.

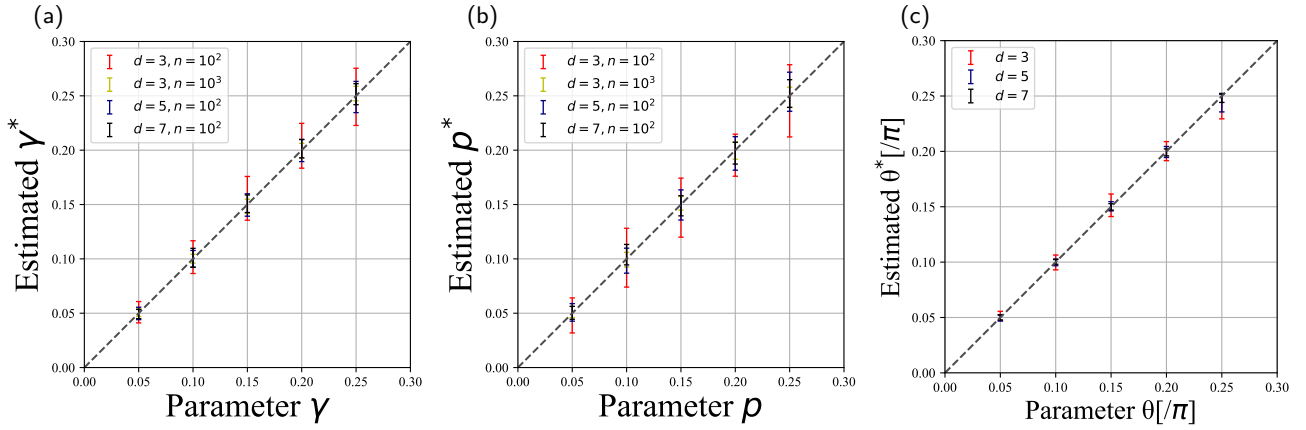


FIG. 4: Results of estimation for the one-parameter uniform noise models: (a) amplitude dumping, (b) phase dumping, and (c) systematic rotation.

### A. Results of Markov chain Monte Carlo for stationary noise models

We explain and discuss the results for the stationary noise models using MCMC explained in Alg. 1. This method is supposed to be used for the calibrations or discussion of estimability.

#### 1. One parameter uniform noise models

First, we show the results for the uniform one-parameter noise model case. We consider the three noise models: amplitude damping (AD), phase damping (de-phase), and systematic rotation (SR) along the  $z$ -axis. These three noise models are described as

$$\begin{aligned} \mathcal{E}_{AD}(\rho) &= K_0 \rho K_0^\dagger + K_1 \rho K_1^\dagger, \\ K_0 &= |0\rangle\langle 0| + \sqrt{1-\gamma}|1\rangle\langle 1|, \\ K_1 &= \sqrt{\gamma}|0\rangle\langle 1|, \end{aligned} \quad (9)$$

$$\begin{aligned} \mathcal{E}_{dephase}(\rho) &= K_0 \rho K_0^\dagger + K_1 \rho K_1^\dagger, \\ K_0 &= |0\rangle\langle 0| + \sqrt{1-p}|1\rangle\langle 1|, \\ K_1 &= \sqrt{p}|1\rangle\langle 1|, \end{aligned} \quad (10)$$

and

$$\mathcal{E}_{SR}(\rho) = e^{-i\theta Z} \rho e^{i\theta Z}, \quad (11)$$

respectively. The size of the surface code is  $d \times d$ , which has the code distance  $d$ , and  $n$  denotes the number of sets of syndrome measurements. In these numerical experiments, the initial state is set to  $\rho_0 \propto |0\rangle_L \langle 0| + |1\rangle_L \langle 1|$ . The estimation results are summarized in Fig. 4.

We set the burn-in time and the total MCMC steps to 500 and  $10^3$ , respectively. Independent estimations for each parameter were performed 20 times for  $d = 7$  and 50 times for the other cases to estimate the sampling bias

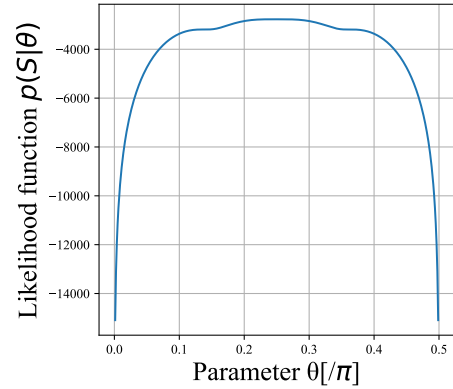


FIG. 5: Likelihood function  $p(\mathbf{S}|\theta)$  of the systematic rotation noise model calculated for the samples  $\mathbf{S} \sim p(\mathbf{S}|\theta = 0.25\pi)$ .

of syndrome measurements. The TN simulator did not use any approximation, so this is the optimal estimation for TN contraction approximation. We find that all the estimations are successful, as seen in Fig. 4. The error bars in the figures mainly represent the sampling bias of syndrome measurements. The size of the error bars should be inversely proportional to the  $\sqrt{n}$ , where  $n$  is the total count of syndrome measurements. We can confirm this behavior in the figures.

The estimation results for the systematic rotation have smaller errors compared with the others. It comes from the difference in noise parameters representing noise models. The range of noise model parameters  $\beta$  of amplitude and phase damping models are  $0 \leq \beta \leq 1$ . On the other hand, the noise model parameter of systematic rotation has cycle  $\pi/2$ . This is why systematic rotation error bars are smaller than the other noise models. Second, for some initial values, the estimation sometimes fails. The reason is that the likelihood function for the systematic rotation noise models is multimodal, as shown

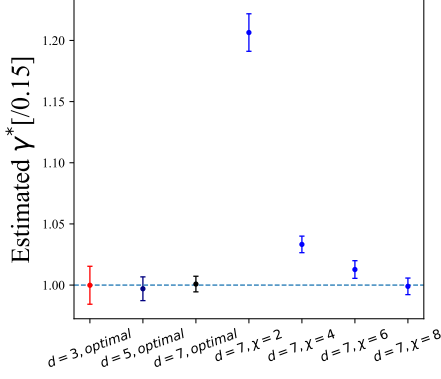


FIG. 6: Dependence of estimation results on code size and maximum bond dimension for amplitude damping with  $\gamma = 0.15$ .

in Fig. 5. The estimation based on the MCMC and EAP estimator is not suitable for multimodal functions. In such situations, we must set the prior distribution to let the posterior distribution be a single modal.

To discuss the accuracy of the tensor network approximation, we did extra experiments for amplitude damping with noise model parameter 0.15. The results are presented in Fig. 6. The number of sets of syndrome measurements is  $n = 10^2$ , and  $\chi$  is the maximum bond dimension for the low-rank approximation of TN contraction. We can see clearly that the larger code has smaller errors. As for the effect of maximum bond dimension, we can see a systematic bias for small  $\chi$ . However, as we increase  $\chi$ , the low-rank approximation becomes more and more accurate, and the bias is negligible for  $\chi = 8$ .

## 2. Two parameter uniform noise models

In this section, we try to estimate the two-parameter noise model cases. We consider the generalized amplitude damping (GAD) and AD+dephase noise models. GAD is defined as

$$\begin{aligned} \mathcal{E}_{GAD}(\rho) &= \sum_{i=0}^3 K_i \rho K_i^\dagger, \\ K_0 &= \sqrt{p}(|0\rangle\langle 0| + \sqrt{1-\gamma}|1\rangle\langle 1|), \\ K_1 &= \sqrt{1-p}(\sqrt{1-\gamma}|0\rangle\langle 0| + |1\rangle\langle 1|), \\ K_2 &= \sqrt{\gamma p}|0\rangle\langle 1|, \\ K_3 &= \sqrt{\gamma(1-p)}|1\rangle\langle 0|, \end{aligned} \quad (12)$$

while AD+dephase is the combination of the amplitude damping and phase damping noise models, and the CPTP map is described as  $\mathcal{E}_{dephase} \circ \mathcal{E}_{AD}(\rho)$ . The results of AD+dephase noise model are shown in Fig. 7. The number of sets of syndrome measurements is  $n = 10^2$ . We can see that the estimation was successful. Naturally, the error bars are larger compared with one-parameter

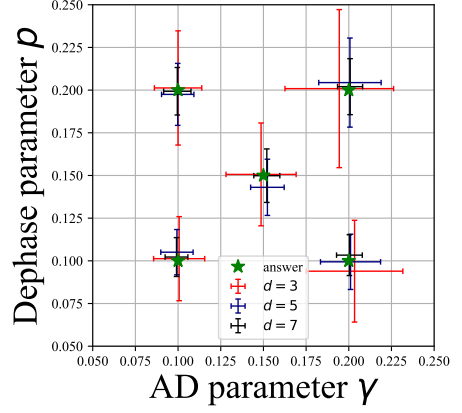


FIG. 7: Results of estimation of the AD+dephase noise model. The green stars in the figures represent the true model parameters.

estimations. We must prepare more syndrome measurement results for multi-parameter estimations to achieve a similar accuracy with the one-parameter case.

Next, we tried to estimate the GAD noise models, but in conclusion, the estimations failed. The results are presented in Fig. 8. We can estimate the parameter dominating the strength of amplitude damping; on the other hand, we cannot estimate the parameter that represents the probability of the transitions of which the directions of damping are from  $|0\rangle$  to  $|1\rangle$  or from  $|1\rangle$  to  $|0\rangle$ . The reason is apparent if we look at Fig. 9, where the landscape of likelihood function is represented by the heatmap. In the AD+dephase case, the likelihood function has a sharp peak; thus, we can estimate the noise parameter accurately. On the other hand, in the GAD case, the dependence of likelihood on  $p$  is tiny. This fact prevents estimating  $p$  reliably even if we optimize the prior distribution. However, from the viewpoint of TN decoding, this may mean that the accuracy of the  $p$  parameter does not significantly impact decoding performance because the computation in the TN decoding process is similar to the calculation of the likelihood function. This is also true for other decoding schemes that use information from the noise model. We conclude that while the estimability generally strongly depends on the noise type, its effect on the decoding performance is not always significant, especially in multi-parameter cases.

## 3. Nonuniform case

Next, we show the results for the nonuniform noise model cases, where the noise model parameter depends on the qubit position. The code size is  $3 \times 3$ , and the target noise model is the nonuniform amplitude noise model with  $\gamma_{ij} = 0.05(3i + j + 1)$  for qubit at  $(i, j)$ . The results are put together in Fig. 10. We can see the estimation of non-uniform noise parameters was successful. How-



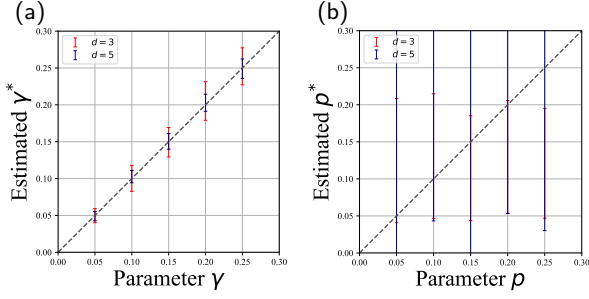


FIG. 8: Results of one parameter estimation for the GAD noise model parameters: (a) Estimation of  $\gamma$  with fixed  $p = 0.1$ . (b) Estimation of  $p$  with fixed  $\gamma = 0.1$ .

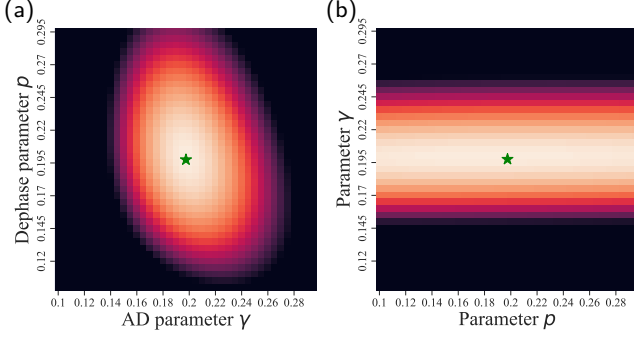


FIG. 9: Heatmaps of likelihood functions  $p(\mathbf{S}|\alpha)$  for (a) AD+dephase and (b) GAD. The code size is  $5 \times 5$ , and the number of syndrome measurement sets  $n$  is  $10^4$ . The green stars represent the true model parameters.

ever, more syndrome measurement results are needed to achieve a similar accuracy as the uniform case, Fig. 4(a).

### B. Results of sequential Monte Carlo for time-varying noise models

In this section, we show the estimation results by using the TN simulator and SMC (Alg. 3) for time-varying noise models, more realistic situations than the previous section.

#### 1. Amplitude damping noise model and the effect for decoder performance

First, we show the results for the time-varying amplitude damping noise models. We choose noise model parameters as a sin-like function as  $\gamma(t) = a(b + \sin(2\pi\omega t))$  with  $a = 0.15$ ,  $b = 1.1$ , and  $\omega = 10^{-4}$ . The posterior distribution is a random walk distribution in Alg. 3. The results are presented in Fig. 11. We can see that the estimated parameters track the time-varying noise model parameter reasonably well. As with previous estimation results, the larger the code size is, the more accurate the estimations are.

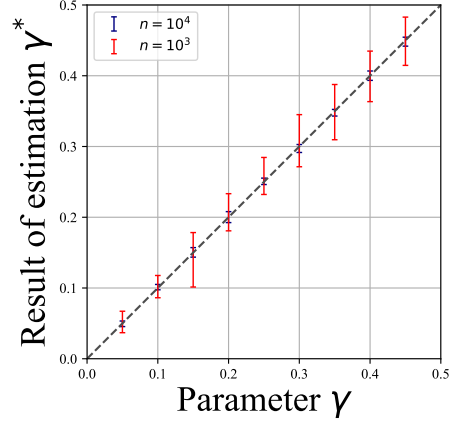


FIG. 10: Results of estimation for nonuniform noise model. The code size is  $3 \times 3$ , and the noise model is the amplitude damping noise model with  $\gamma_{ij} = 0.05(3i + j + 1)$  for qubit at  $(i, j)$ .

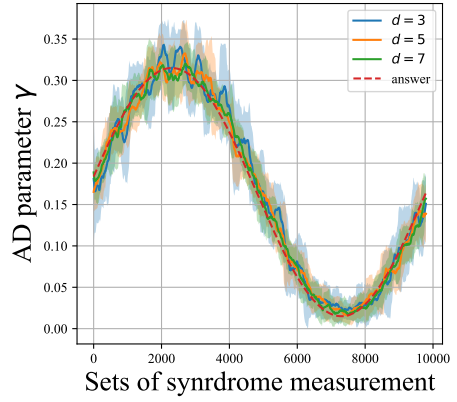


FIG. 11: Results of estimation using SMC of sin-like time-varying noise model parameter of amplitude damping. The color range represents fluctuation before the smoothing process. The number of particles is  $N = 128$ , the resampling interval is  $T = 10$ , and the smoothing time is  $t = 20$ . The contraction of the TN is taken exactly.

Next, we consider the line-like time-varying noise model and discuss the influence of estimations on decoding performance. The noise model parameter is taken as  $\gamma(t) = a + bt$  with  $a = 0.2$  and  $b = 10^{-5}$ . The estimation results are shown in Fig. 12.

We can see that the estimations can track the time-varying noise parameter very well. Using the estimation results, we can achieve performance comparable to the optimal decoding. To claim the need for estimation beyond the Pauli noise models, we also perform the estimation assuming the Pauli noise models. We can see that the decoding performance of the main method is better than that of the Pauli noise models. Thus, we conclude that selecting the appropriate noise model is important

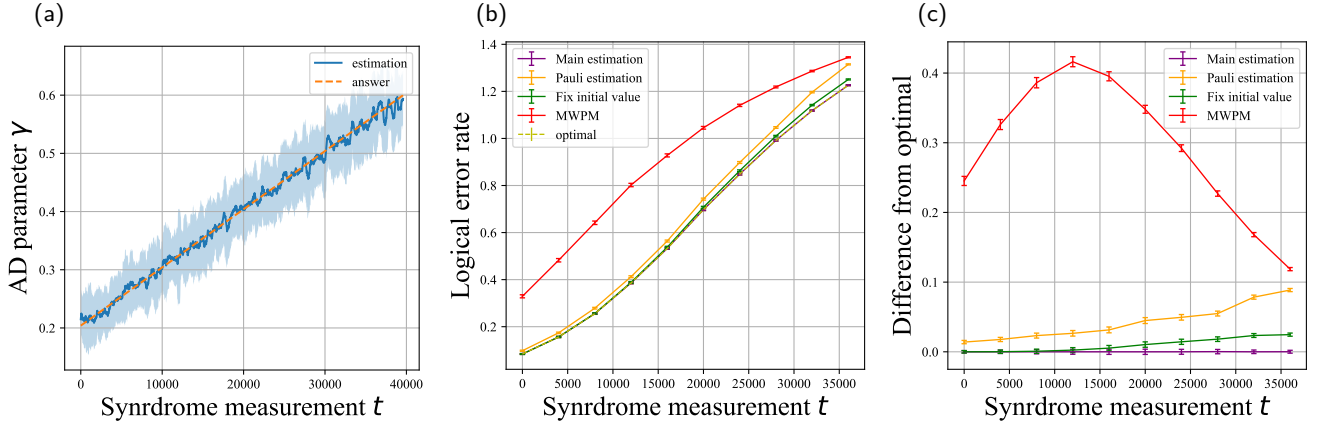


FIG. 12: Results of estimation for line-like time-varying noise model and decode performance for (a) code size  $5 \times 5$ , the number of particles  $N = 2560$ , resampling interval  $T = 10$ , smoothing time  $t = 40$ . (b) Decode performance of  $7 \times 7$  code for five patterns, which is calculated for  $10^3$  samples: (purple) estimation result, (yellow) estimation result assuming Pauli noise models, (green) estimation using the initial noise model parameter  $\gamma = 0.2$ , (red) MWPM decode results, (dotted) optimal decoding. (c) Difference of decode performance from the optimal result. TN simulations do not use any approximation.

for decoding performance. To select the noise model, we must remember that some noise models, such as the GAD noise models, cannot be estimated.

## 2. Nonuniform case

Our SMC estimator method is expected to work well for estimating multi-parameter noise models as the MCMC estimator. In this section, we present the results for the nonuniform line-like noise models. The noise model is set as  $\gamma_{ij}(t) = a(3i + j + 1) + bt$  with  $a = 0.05$  and  $b = 10^{-6}$  for qubit at  $(i, j)$ . The results are shown in Fig. 13. We can see that the noise model is estimated successfully.

## V. SUMMARY AND FUTURE ISSUES

In this paper, we propose novel noise model estimation methods based on syndrome measurement results using the TN and Monte Carlo methods. As seen in Sec. IV, the proposed methods work well for various noise models. The TN simulator of the surface code can efficiently simulate arbitrary noise models for physical qubits. Thus, the proposed estimation method can be applied to a broader range of noise models than just the Pauli noise models. This work is expected to broaden the study of decoding algorithms that utilize general noise models, thereby accelerating the realization of fault-tolerant quantum computing.

The proposed methods are based on Bayesian inference. Thus, even when the assumed noise model differs from the actual noise model in the device, the estimation can still work, and its outcomes are evaluated probabilis-

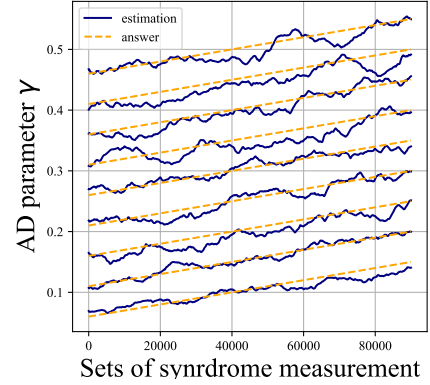


FIG. 13: Results of estimation for time-varying nonuniform noise model case. Each line denotes the results for each qubit. The code size is  $3 \times 3$ , and the noise models are the amplitude damping noise models whose parameters are  $\gamma_{ij}(t) = a(3i + j + 1) + bt$  with  $a = 0.05$  and  $b = 10^{-6}$  for qubit at  $(i, j)$ . TN simulations do not use any approximation.

tically. It is one of the advantages of using Bayesian inference not found in point estimations. While the proposed methods, in principle, can apply to arbitrary noise models, we found that some noise models, such as the generalized amplitude damping, cannot be estimated. It is natural because the estimations are based on the syndrome measurement results that cannot give us complete information about the quantum process. From the perspective of the efficiency of surface code decoding, however, this may not be a disadvantage as the estimability of the noise model is closely linked to the significance

of the information provided by the noise model in the decoding process.

Several factors determine the estimation accuracy in the proposed noise model estimation schemes. One is the statistical fluctuation in the posterior distribution due to the finite number of samples of the syndrome measurements. The second is the statistical error resulting from the finite Monte Carlo steps in MCMC and the finite number of particles in SMC. The last is the systematic bias from the low-rank tensor approximation. We must appropriately optimize the hyperparameters to achieve accurate estimations. However, we can eliminate the last one, the systematic bias in tensor approximation, by using the Monte Carlo sampling in tensor network contraction [56]. Our proposed estimation methods have already been developed by combining the TN and Monte Carlo techniques. Thus, integrating the tensor network Monte Carlo sampling method into our framework must be straightforward.

It should also be noted that the surface code TN simulator assumes that the syndrome measurement process is noise-free. In realistic scenarios, consideration of such measurement errors is crucial. We must improve or develop new methods for computing the likelihood function to address this issue.

There is still some room to improve our methods. For MCMC methods, the estimations sometimes fail when the likelihood function is multimodal. To deal with this difficulty, we can employ advanced sampling methods, such as the exchange Monte Carlo method [57, 58]. For the SMC methods, we currently use the random walk distribution for the proposed distribution. If the proposed distributions catch the time-varying trend more, the estimations will be more accurate.

As for the estimation time, Monte Carlo simulations

generally take a long time. It is possible to shorten the estimation time by parallelizing the likelihood calculation, distributing SMC particles to many computation nodes, and introducing efficient low-rank approximation in the TN method. However, it may not be enough for practical QEC, as the decoding time should be shorter than the decoherence time. There might be two options to overcome such difficulties. One is to utilize a subset of the syndrome measurement results instead of the entire dataset, effectively thinning out the data. Another is to restrict our simulation code size and divide the results of syndrome measurements. If the noise models can be estimated accurately for a smaller code, e.g.,  $3 \times 3$ , dividing the measurement results can accelerate the TN simulation and improve the performance by using parallelization.

Finally, as demonstrated in Fig. 12, the choice of noise model itself is more important than the accuracy of noise model parameter estimation for the decode performance of the TN decoder. By generalizing the present Bayesian inference scheme, the noise model selection may become possible [59, 60].

## ACKNOWLEDGMENTS

This work was supported by the Center of Innovation for Sustainable Quantum AI, JST Grant Number JPMJPF2221, and JSPS KAKENHI Grant Numbers 20H01824 and 24K00543. TK acknowledges the support of JST SPRING Grant Number JPMJSP2108. The computation in this work has been partially done using the AI cluster system at the Institute for Physics of Intelligence, the University of Tokyo, and the facilities of the Supercomputer Center, the Institute for Solid State Physics, the University of Tokyo.

- 
- [1] R. P. Feynman, *International Journal of Theoretical Physics* **21**, 467 (1982).
  - [2] M. A. Nielsen and I. L. Chuang, *Quantum computation and quantum information* (Cambridge university press, 2010).
  - [3] P. W. Shor, *SIAM Review* **41**, 303 (1999).
  - [4] A. W. Harrow, A. Hassidim, and S. Lloyd, *Physical Review Letters* **103**, 150502 (2009).
  - [5] G. H. Low and I. L. Chuang, *Physical Review Letters* **118**, 010501 (2017).
  - [6] A. Steane, *Proc. Roy. Soc. Lond.* **452**, 2551–2577 (1996).
  - [7] A. Kitaev, *Annals of Physics* **303**, 2 (2003).
  - [8] S. B. Bravyi and A. Y. Kitaev, arXiv preprint (1998), [arXiv:quant-ph/9811052 \[quant-ph\]](#).
  - [9] E. Dennis, A. Kitaev, A. Landahl, and J. Preskill, *Journal of Mathematical Physics* **43**, 4452 (2002).
  - [10] S. Krinner, N. Lacroix, A. Remm, A. Di Paolo, E. Genois, C. Leroux, C. Hellings, S. Lazar, F. Swiadek, J. Hermann, G. J. Norris, C. K. Andersen, M. Müller, A. Blais, C. Eichler, and A. Wallraff, *Nature* **605**, 669 (2022).
  - [11] Google Quantum AI, *Nature* **614**, 676 (2023).
  - [12] D. Bluvstein, S. J. Evered, A. A. Geim, S. H. Li, H. Zhou, T. Manovitz, S. Ebadi, M. Cain, M. Kalinowski, D. Hangleiter, J. P. Bonilla Ataides, N. Maskara, I. Cong, X. Gao, P. Sales Rodriguez, T. Karolyshyn, G. Semeghini, M. J. Gullans, M. Greiner, V. Vuletić, and M. D. Lukin, *Nature* **626**, 58–65 (2023).
  - [13] S. T. Spitz, B. Tarasinski, C. W. J. Beenakker, and T. E. O’Brien, *Adv. Quantum Technol.* **1**, 1800012 (2018).
  - [14] S. Huang, M. Newman, and K. R. Brown, *Phys. Rev. A* **102**, 012419 (2020).
  - [15] C. T. Chubb, arXiv preprint (2021), [arXiv:2101.04125 \[quant-ph\]](#).
  - [16] A. S. Darmawan and D. Poulin, *Phys. Rev. E* **97**, 051302 (2018).
  - [17] J. P. Bonilla Ataides, D. K. Tuckett, S. D. Bartlett, S. T. Flammia, and B. J. Brown, *Nat. Commun.* **12**, 2172 (2021).
  - [18] D. K. Tuckett, S. D. Bartlett, and S. T. Flammia, *Phys. Rev. Lett.* **120**, 050505 (2018).
  - [19] A. Dua, A. Kubica, L. Jiang, S. T. Flammia, and M. J. Gullans, Clifford-deformed surface codes (2023),

- [arXiv:2201.07802 \[quant-ph\]](#).
- [20] A. S. Darmawan and D. Poulin, *Phys. Rev. Lett.* **119**, 040502 (2017).
  - [21] I. L. Chuang and M. A. Nielsen, *Journal of Modern Optics* **44**, 2455 (1997).
  - [22] T. Evans, W. Huang, J. Yoneda, R. Harper, T. Tanttu, K. Chan, F. Hudson, K. Itoh, A. Saraiva, C. Yang, A. Dzurak, and S. Bartlett, *Phys. Rev. Appl.* **17**, 024068 (2022).
  - [23] Y. Fujiwara, arXiv preprint (2014), [arXiv:1405.6267 \[quant-ph\]](#).
  - [24] A. G. Fowler, arXiv preprint (2014), [arXiv:1307.1740 \[quant-ph\]](#).
  - [25] T. Wagner, H. Kampermann, D. Bruß, and M. Kliesch, *Phys. Rev. Research* **3**, 013292 (2021).
  - [26] T. Wagner, H. Kampermann, D. Bruß, and M. Kliesch, *Quantum* **6**, 809 (2022).
  - [27] M.-X. Huo and Y. Li, *New J. Phys.* **19**, 123032 (2017).
  - [28] J. Kelly, R. Barends, A. G. Fowler, A. Megrant, E. Jeffrey, T. C. White, D. Sank, J. Y. Mutus, B. Campbell, Y. Chen, Z. Chen, B. Chiaro, A. Dunsworth, E. Lucero, M. Neeley, C. Neill, P. J. J. O'Malley, C. Quintana, P. Roushan, A. Vainsencher, J. Wenner, and J. M. Martinis, *Phys. Rev. A* **94**, 032321 (2016).
  - [29] S. Aaronson and D. Gottesman, *Phys. Rev. A* **70**, 052328 (2004).
  - [30] C. Gidney, *Quantum* **5**, 497 (2021).
  - [31] J. J. Wallman and J. Emerson, *Phys. Rev. A* **94**, 052325 (2016).
  - [32] A. P. Dempster, N. M. Laird, and D. B. Rubin, *Journal of the royal statistical society: series B (methodological)* **39**, 1 (1977).
  - [33] T. Bayes, *Philosophical transactions of the Royal Society of London*, 370 (1763).
  - [34] N. Metropolis, A. W. Rosenbluth, M. N. Rosenbluth, A. H. Teller, and E. Teller, *jcp* **21**, 1087 (1953).
  - [35] S. Chib and E. Greenberg, *The american statistician* **49**, 327 (1995).
  - [36] W. K. Hastings, *Biometrika* **57**, 97 (1970).
  - [37] G. Kitagawa, in *Proceedings of the 2nd US-Japan joint seminar on statistical time series analysis*, Vol. 2 (1993) pp. 110–131.
  - [38] A. Doucet, N. De Freitas, N. J. Gordon, *et al.*, *Sequential Monte Carlo methods in practice*, Vol. 1 (Springer, 2001).
  - [39] D. Gottesman, Stabilizer codes and quantum error correction (1997), [arXiv:quant-ph/9705052 \[quant-ph\]](#).
  - [40] L. Rieseboos, X. Fu, S. Varsamopoulos, C. G. Almudever, and K. Bertels, in *Proceedings of the 54th Annual Design Automation Conference 2017* (2017) pp. 1–6.
  - [41] H. Bombin and M. A. Martin-Delgado, *Phys. Rev. A* **76**, 012305 (2007).
  - [42] R. Orús, *Nature Reviews Physics* **1**, 538 (2019).
  - [43] F. Verstraete and J. I. Cirac, arXiv preprint (2004), [arXiv:cond-mat/0407066 \[cond-mat.str-el\]](#).
  - [44] U. Schollwöck, *Annals of Physics* **326**, 96 (2011).
  - [45] M. Katsuda, K. Mitarai, and K. Fujii, arXiv preprint (2022), [arXiv:2204.11404 \[quant-ph\]](#).
  - [46] A. S. Darmawan, Optimal adaptation of surface-code decoders to local noise (2024), [arXiv:2403.08706 \[quant-ph\]](#).
  - [47] N. J. Gordon, D. J. Salmond, and A. F. Smith, in *IEE proceedings F (radar and signal processing)*, Vol. 140 (IET, 1993) pp. 107–113.
  - [48] G. Kitagawa, *J Comput Graph Stat* **5**, 1 (1996).
  - [49] J. Carpenter, P. Clifford, and P. Fearnhead, *IEE Proceedings-Radar, Sonar and Navigation* **146**, 2 (1999).
  - [50] E. R. Beadle and P. M. Djuric, *IEEE Transactions on Aerospace and Electronic Systems* **33**, 338 (1997).
  - [51] J. S. Liu and R. Chen, *J Am Stat Assoc* **93**, 1032 (1998).
  - [52] R. Douc, O. Cappé, and É. Moulines, *ISPA 2005. Proceedings of the 4th International Symposium on Image and Signal Processing and Analysis*, 2005., 64 (2005).
  - [53] T. Li, M. Bolic, and P. M. Djuric, *IEEE Signal processing magazine* **32**, 70 (2015).
  - [54] N. J. Gordon, D. J. Salmond, and A. F. Smith, in *IEE proceedings F (radar and signal processing)*, Vol. 140 (IET, 1993) pp. 107–113.
  - [55] A. Doucet, S. Godsill, and C. Andrieu, *Statistics and computing* **10**, 197 (2000).
  - [56] A. J. Ferris, arXiv preprint (2015), [arXiv:1507.00767 \[cond-mat.stat-mech\]](#).
  - [57] R. H. Swendsen and J.-S. Wang, *Phys. Rev. Lett.* **57**, 2607 (1986).
  - [58] K. Hukushima and K. Nemoto, *Journal of the Physical Society of Japan* **65**, 1604 (1996), <https://doi.org/10.1143/JPSJ.65.1604>.
  - [59] D. Madigan and A. E. Raftery, *J Am Stat Assoc* **89**, 1535 (1994).
  - [60] A. E. Raftery, D. Madigan, and J. A. Hoeting, *J Am Stat Assoc* **92**, 179 (1997).